Restoring three-dimensional magnetic resonance angiography images with mean curvature motion

Claudia Schlimper*[†], Oliver Nemitz[‡], Ulrich Dorenbeck[§], Jasmin Scorzin*,
Ross Whitaker[¶], Tolga Tasdizen[¶], Martin Rumpf[‡] and Karl Schaller*[#]

*Department of Neurosurgery, University of Bonn Medical Center, Bonn, Germany
[†]Department of Neurosurgery, Hospital Cologne, Cologne, Germany
[‡]Institute for Numerical Simulation, University of Bonn, Bonn, Germany
[§]Department of Radiology, University of Bonn Medical Center, Bonn, Germany
[¶]Scientic Computing and Imaging Institute, University of Utah, Salt Lake City, UT, USA
[#]Department of Neurosurgery, Geneva University Medical Center, Faculty of Medicine, University of Geneva, Geneva, Switzerland

Objective: The management of neurovascular disease requires precise information on the cerebral vascular anatomy. Digital subtraction angiography (DSA) is the gold standard against which other imaging modalities have to be measured. To improve the quality of three-dimensional (3D) magnetic resonance angiography (MRA) images, we present a novel concept in 3D image analysis.
Methods: Five patients, harboring cerebral aneurysm, underwent DSA, computed tomography angiography (CTA) and MRA. MRA data were processed using a novel anisotropic curvature motion model. Three-dimensional reconstructions of CTA and MRA datasets were used for comparison.
Results: The 3D-reconstructed images accurately displayed all aneurysms. The anatomy of the anterior part of the circle of Willis was visualized reliably. The smoothened vessel surfaces enhanced the readability of the images. Regarding visual representation of the posterior part of the circle of Willis, the post-processed MRA showed the arterial segments less accurate than the standard modalities.
Conclusions: This new approach is a promising tool for planning of neurovascular interventions and preoperative evaluation.

Keywords: Anisotropic geometric diffusion, cerebral aneurysm, 3D-reconstructed image, magnetic resonance angiography, tubular structures

Objectives

The management of neurovascular disease requires precise information on vascular anatomy, e.g. visualization of cerebral arteries, veins and distinct pathoanatomical variations (e.g. fenestration, aneurysm and others). Digital subtraction angiography (DSA) is still considered the gold standard for the diagnosis and radiographic analysis of cerebral aneurysms with its main advantage being its high spatial image resolution. It is the standard by which other imaging modalities are validated to assess their capacity to visualize intracranial vascular lesions[1]. The invasive nature of DSA is a disadvantage, however, carrying an approximate 0·5% rate of persistent neurological complications and a 1% risk related to complications from arterial puncture and catheter manipulation[2–5]. Furthermore, depending on vascular status, DSA can be time-consuming, and it provides a two-dimensional (2D) depiction of three-dimensional (3D) anatomy only.

Computed tomography angiography (CTA) and magnetic resonance angiography (MRA) are non-invasive imaging techniques of cerebral vessels. CTA images can be obtained within a few minutes by a trained technician and the CTA data can be viewed from unlimited projections in both 2D and 3D, thus facilitating aneurysm detection and characterization[6,7]. Currently, these obvious advantages have to be weighed against a supposedly lower visuospatial resolution when compared with DSA despite considerable recent developments in computer hardware and software, which create a more user-oriented computational environment. For example, turbulent flow within the aneurysm may cause poor visualization of the aneurysm with MRA and thus lead to unreliable judgement with regard to its angioarchitectural and topographical relationship with adjacent arteries or those originating from the aneurysm[8].

Ideally, one would be able to visualize the 3D topographical and angioarchitecture in a given

patient with neurovascular disease for assessment of therapeutic options and associated risks before endovascular or surgical treatment. Three-dimensional-reconstructed images and the possibility for image rotation are very valuable in preoperative planning and preparation. To improve the quality of the 3D-reconstructed images, we discuss a novel concept in 3D image analysis for the cerebral arterial tree. The concept is based on template-driven anisotropic geometric diffusion for subsequent segmentation of blood vessels from medical images, and it is compared with the results from 'conventionally' processed MRA and CTA images as well as against gold standard DSA[9]. The particular emphasis of this paper is on the validation.

Methods

Five patients with intracranial aneurysms were enrolled in this study; two patients presented with subarachnoid hemorrhage (SAH) and the remaining three had incidental intracranial aneurysms. All patients were evaluated by multislice CTA, DSA and MRA.

CTA data acquisition

CTA was performed on a multislice 16-row CT scanner Tomoscan SR 7000 (Philips Medical System, Eindhoven, The Netherlands). The gantry was unangled, starting at the level of sphenoid sinus. Using an 18-gauge needle into a peripheral arm vein, injection of 80 ml non-ionic contrast material (Jodutrast, Jopamidol Solutrast 370 mg/l; Altana Pharma, Konstanz, Germany) and injection of 50 ml sodium chloride were performed using a power injector at a rate 4–5 ml/s. To individualize the timing of contrast material injection, automatic bolus tracking techniques were used. Scanning parameters were 90 kV, 300 mAs and rotation time 0·5 seconds. Axial images (1 mm thickness) at 0·5 mm increments were acquired (0·688 pitch).The datasets were acquired with $16 \times 0·75$ mm detector collimation. Further scanning parameters included 240 mm field of view (FOV) and a 512×512 matrix. The source images were post-processed using maximum intensity projection (MIP) and multiplanar reconstruction (MPR). Voxel-rendering techniques allow a 3D display of the vessels.

Digital subtraction angiography

All five patients were examined with intracranial catheter angiography using the Seldinger technique and percutaneous catheterization of the femoral artery. Anteroposterior, lateral and oblique views were routinely obtained.

Selective catheterizations were performed in both internal carotid and vertebral arteries. The arteries were visualized by contrast injection. Contrast material was injected manually with a volume of 7–9 ml.

Magnetic resonance imaging and 3D time-of-flight MRA

Routine 3D time-of-flight (TOF) MRA sequences were obtained using a 3 T scanner (3 T, Intera; Philips Medical Systems, Best, The Netherlands) with

the following parameters: TR 25 ms, TE 3·45 ms (out-phase), flip angle 20°, scan matrix 528, NSA 1, FOV 200 mm, one slab, 20 mm slab thickness, 0·5 mm effective slice thickness, using the sense head coil.

With parallel imaging technique, sagittal and axial T1-FFE-sequences were taken to evaluate the intracranial structures. The study was completed by 3D-TOF acquisition covering an area from the clivus to the genu of corpus callosum.

The images were transferred to the workstation (BrainLAB, Heimstetten, Germany) in DICOM format. The viewing projection for the perspective image was indicated by arrows on the source axial image, the coronal and sagittal reconstructions, and the 3D volume-rendering image.

Restoring 3D MRA images based on template-driven anisotropic geometric diffusion

For details on the mathematical background from geometry and the relevant background on geometric partial equations, we refer to Nemitz *et al*[9].

The basis of our method is an anisotropic version of the so-called mean curvature flow. Isotropic mean curvature flow is the gradient flow corresponding to surface area[10].

Indeed each point of a surface M will move with a certain velocity (the speed actually turns out to be the mean curvature of the surface) such that the surface area is reduced fastest. Consequently, every closed convex surface will continuously shrink until it disappears and up to scaling the evolving surface will tend towards a sphere.

Considering an anisotropic area functional

$$e[M] = \int_M \gamma(n)\,\mathrm{d}a$$

it is possible to weigh surface area locally depending on the orientation[8].

Here, surface orientation is expressed by the normal vector n on the surface M. In the case where $\gamma(\cdot)$ is the 2-norm, the integrant is constant for any surface orientation and we obtain the usual isotropic surface area[11].

Gradient flows of this modified surface area converge up to scaling to different shapes, the so-called Wulff shapes, determined by the choice of the anisotropy γ. This type of flow is denoted anisotropic mean curvature flow[9,12,13]. In our method, we choose elongated ellipsoids as Wulff shapes. These Wulff shapes serve as suitable local priors for a ventricle and reflect the underlying tubular structure. To avoid a shrinking of the surface, the velocity is modified in such a way that the volume of the surface is approximately conserved[9,14].

The reconstruction algorithms based on this concept works as follows: First, the vessels from the original image are extracted. This is carried out by a simple thresholding[9].

Second, the orientations of the vessels have to be computed to align the ellipsoids to the vessels. This is carried out with a moment analysis. Thus, the structure tensor

$$M_V(x_0) :=$$

$$\frac{1}{m_v(x_0)} \int_{B_{r(x_0)}} X_V(x)[x - C_V(x_0)] \otimes [x - C_V(x_0)] dx$$

is computed for each point of the 3D MRA image. Here, X_v is the characteristic function for the vessel structures V, $m_v(x_0)$ is the mass and $C_V(x_0)$ the center of gravity of the distribution X_V.

The eigenvalues and eigenvectors of this tensor provide information about the orientation of the vessels[14].

The eigenvector belonging to the largest eigenvalue is the direction of the vessel and the ratio between the largest and the second largest eigenvalue is a reliable indicator for elongated structures. For the computation of the structure tensor, the radius R of the spherical integration domain $B_{R(x)}$ has to be defined. Based on the computation of the zero moment for two different radii, we are able to identify approximately tubular vessels and estimate their radius. The radius of the integration domain is then considered as a multiple of this estimated vessel radius.

Then, for each image point which is classified as closed to a ventricle, a Wulff shape W_x is defined as a properly elongated ellipsoid. Again, based on the prior moment analysis, the Wulff shape is properly rotated into the orientation of the vessel. To this family of spatially varying Wulff shapes W_x, we consider a corresponding family of anisotropic area integrants $\gamma_x(\cdot)$ and define the inhomogeneous, anisotropic surface area.

Finally, the resulting anisotropic mean curvature motion leads to a suitable denoising of tubular vessel structures. Furthermore, we are able to restore corrupted vessel structures. Indeed, smaller gaps are closed via growth of the opposite ends of the vessel towards each other (*Figure 1*).

The final gradient flow is discretized with linear finite elements in space and with a semi-implicit backward Euler discretization in time. To reduce the amount of computation, we define a narrow band[15] around the vessels where computation is performed.

Figure 1 (Left) Oriented ellipsoid overlaying a test geometry; the ellipsoid has to be rotated into the orientation of the blood vessel at each point. (Right) Processing of the vessel geometry

The following parameters were recorded and compared among the four methods with DSA as gold standard, CTA, MRA and the new template-driven approach:

- the presence of all intracerebral vessels by assessment of the circle of Willis and their structural appearance;
- the presence or absence of aneurysms;
- in case of an aneurysm, its location, size, shape, neck diameter, orientation of its dome, and its relationship with parent vessels, transitory vessels and vessels originating from the aneurysm itself.

Results

Five patients, ranging in age from 43 to 62 years (mean age: 53 years), were evaluated for intracranial aneurysms. Two patients suffered from SAH and three patients had unruptured intracranial aneurysms. Four of the five patients underwent MRA, CTA and DSA. One patient had MRA only. We calculated sensitivities for the MR angiographic MIP images and post-processed images, taking DSA as the standard of reference and considering partially visible arterial segments as present. The number of arterial segments determined to be visible, partially visible, or not visible on each of the imaging techniques is summarized in *Table 1* and *Figures 2–6*.

Intraarterial angiography depicted 20 vessel segments as presented and 0 as absent. The MRA MIP images correctly showed 22 of 25. There were one

Table 1 Segments of the circle of Willis and of aneurysms. The number of arterial segments of the five patients determined to be present, partially present or not present on each of the imaging techniques, is summarized in this table (four patients were evaluated by DSA, CTA and MRA. One patient underwent only MRA)

Artery	Intraarterial DSA			CTA MIP images			MRA MIP images			Post-processed MRA		
	Present	Absent	Partially present	Present	Absent	Partially present	Present	Absent	Partially present	Present	Absent	Partially present
Anterior communicating	4 (4)		3 (4)	1 (4)		5 (5)			5 (5)			
Posterior communicating	4 (4)		2 (4)	2 (4)		3 (5)	1 (5)	1 (5)	2 (5)	1 (5)		2 (5)
Anterior cerebral (A1 segment)	4 (4)		4 (4)			4 (5)		1 (5)	4 (5)			1 (5)
Middle cerebral (M1 segment)	4 (4)		4 (4)			5 (5)			5 (5)			
Posterior cerebral (P1 segment)	4 (4)		3 (4)	1 (4)		5 (5)			5 (5)			
Aneurysm	4 (4)		4 (4)			4 (5)	1 (5)		4 (5)			1 (5)

DSA: digital subtraction angiography; CTA: computed tomographic angiography; MRA: magnetic resonance angiography; MIP: maximum intensity projection.
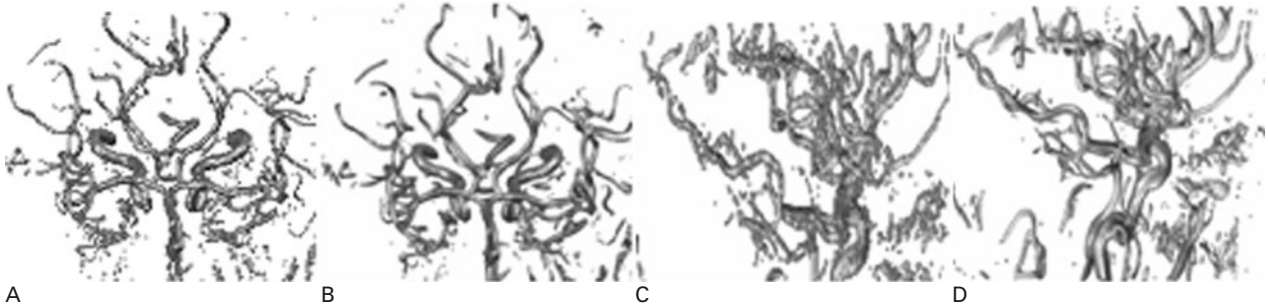
Figure 2 MIP images of the circle of Willis in a patient with an aneurysm of posterior communicating artery on the left side. The female patient (62 years old) had ICB. (A and C) MIP images of conventional MRA; (B and D) MIP images of post-processed MRA; (A and B) axial, superior view; (C and D) lateral view of MIP image
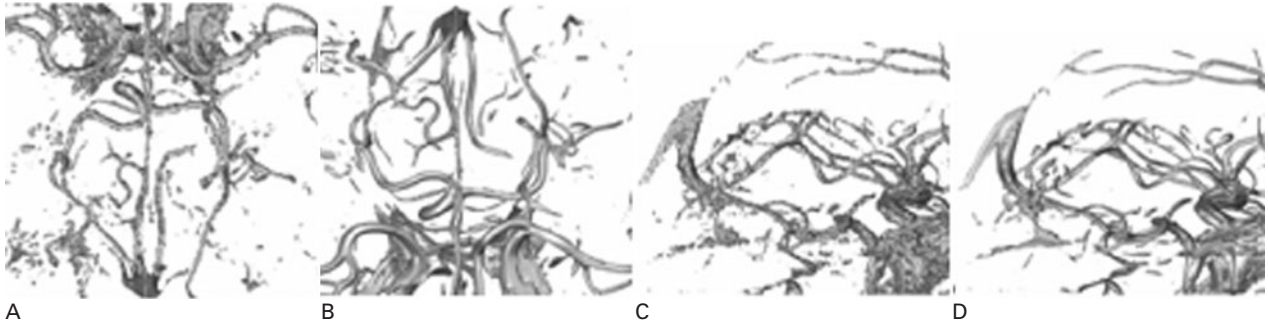
Figure 3 MIP images of the circle of Willis in a patient with a small aneurysm of anterior communicating artery. The patient (43 years old) had SAH H&H II. (A and C) MIP images of conventional MRA; (B and D) MIP images of post-processed MRA; (A and B) axial, superior view; (C and D) lateral view of MIP image
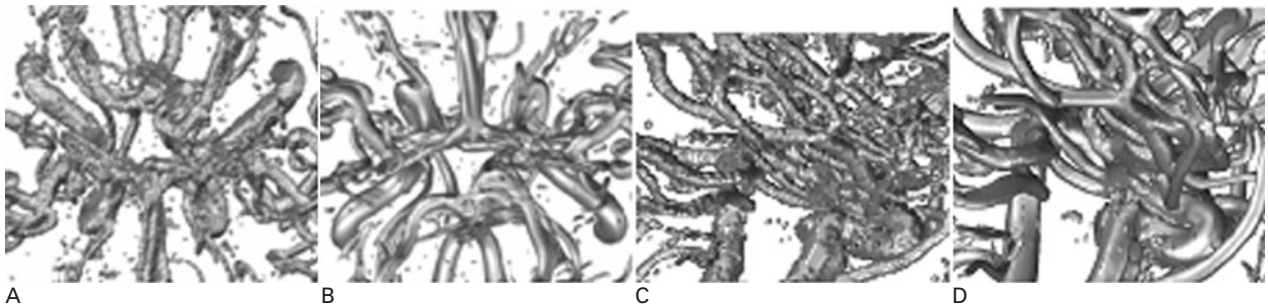
Figure 4 MIP images of the circle of Willis in a male patient (52 years old) with an incidental aneurysm of the anterior communicating artery. (A and C) MIP images of conventional MRA; (B and D) MIP images of post-processed MRA; (A and B) axial, superior view; (C and D) lateral view of MIP image

Figure 5 MIP images of the circle of Willis in a male patient (55 years old) with an incidental aneurysm of the anterior communicating artery. (A and C) MIP images of conventional MRA; (B and D) MIP images of post-processed MRA; (A and B) axial, superior view; (C and D) lateral view of MIP image

segment absent and two segments partially present. Subgroup analysis of the anterior vessel complex and posterior vessel complex of the circle of Willis showed a sensitivity of 93% of the anterior vessel complex and a sensitivity of 80% of the posterior vessel complex (*Table 1*).
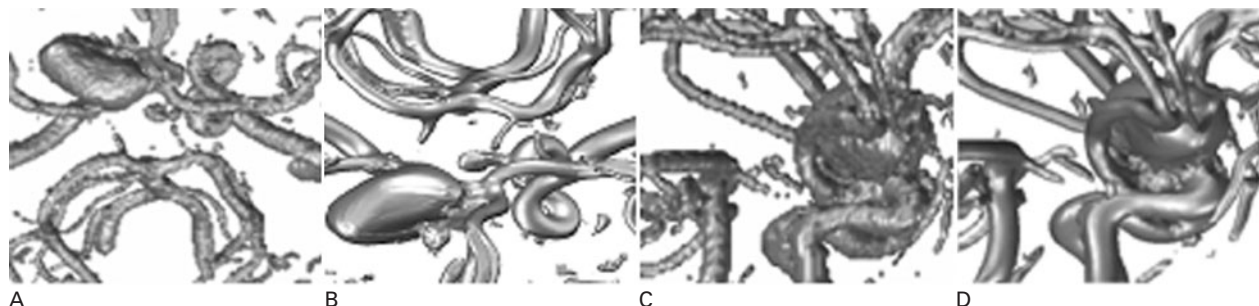
Figure 6 **MIP images of the circle of Willis in a female patient (58 years old) with an incidental aneurysm of the anterior communicating artery.** (A and C) **MIP images of conventional MRA;** (B and D) **MIP images of post-processed MRA;** (A and B) **axial, superior view;** (C and D) **lateral view of MIP image**

The post-processed MRA data could visualize the anterior vessel complex of the circle of Willis reliable as compared with DSA. Surgical anatomy of the anterior part of the circle of Willis was delineated with an improved visuospatial orientation by the post-processed MRA than by the three standard modalities shown in *Figure 7*.

The sensitivity of post-processed MRA in displaying the anterior vascular complex was 93% equal to the MRA–MIP images (14 vessel segments are presented and one vessel segment is partially presented).

Regarding visual representation of the posterior part of the circle of Willis, the post-processed MRA showed that the arterial segments were less accurate than the standard modalities, DSA, CTA and conventional MRA, which lend to an overall sensitivity of post-processed MRA of 70% in comparison with 80% sensitivity of MRA–MIP images (seven vessel segments were presented, one vessel segment was absent and two segments were partially presented) shown in *Table 1*.

In one case, the posterior communicating artery aneurysm could not reliably be detected by the post-processed MRA in comparison to DSA, CTA and conventional MRA, where it was visualized. After the post-processing of the MRA data, the aneurysm and the internal carotid artery (ICA) became merged

because of the small distance between the ICA and aneurysm (*Figure 8*).

Discussion

Computed tomographic angiography and MRA provide several advantages over DSA. These include reduced cost, avoidance of arterial injury and stroke, rapid image acquisition and the possibility of post-processing of the data[6]. Conventional DSA is the standard manner by which all other less invasive imaging modalities are compared to assess their capacity to visualize intracranial vascular anatomy[16].

We compared the MIP images of TOF MR angiographic sequences, the post-processed images of MRA and MIP images of CTA with findings of intra-arterial DSA, which was the standard of reference, obtained in the same patients. MIP images showed an acceptable sensitivity of 88% regarding visualization of the neurovascular anatomy of the circle of Willis. The sensitivity for accurate visualisation of the anterior vessel complex was 93% with the new MRA post-processing method, but only 80% for the visual representation of the posterior part of the circle of Willis.

Thus, the post-processed MRA of the anterior vessel complex reached the same sensitivity like conventionally processed MRA. Thereby, in addition, the visuospatial resolution of the anterior vessel
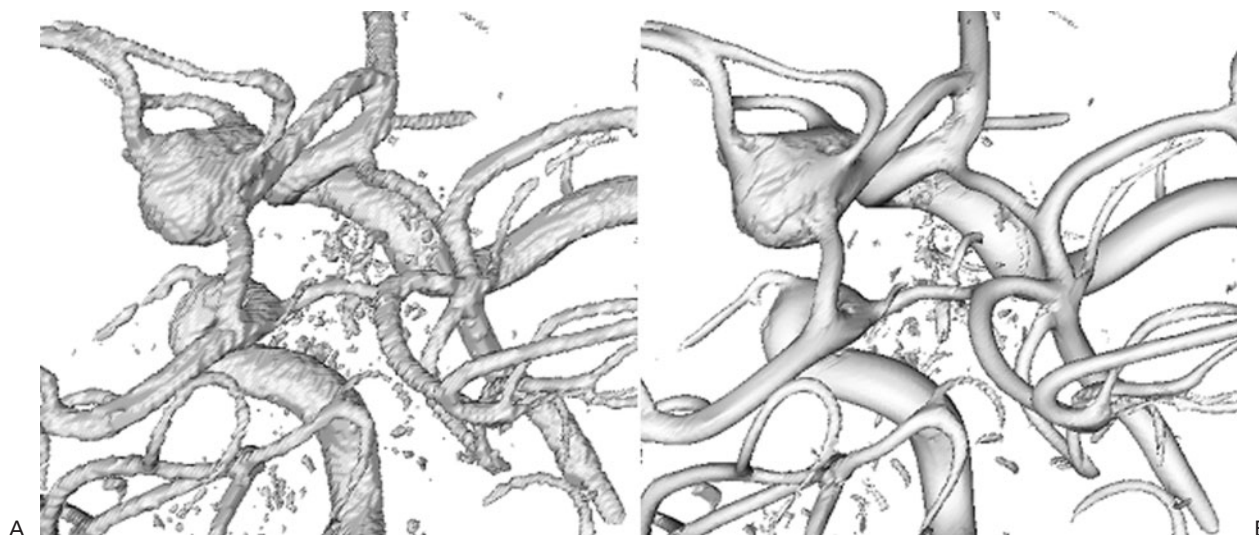
Figure 7 **MIP images of the circle of Willis in a male patient (55 years old) with an incidental aneurysm of the anterior communicating artery.** (A) **MIP images of conventional MRA (superior, oblique view);** (B) **MIP images of post-processed MRA (superior, oblique view)**
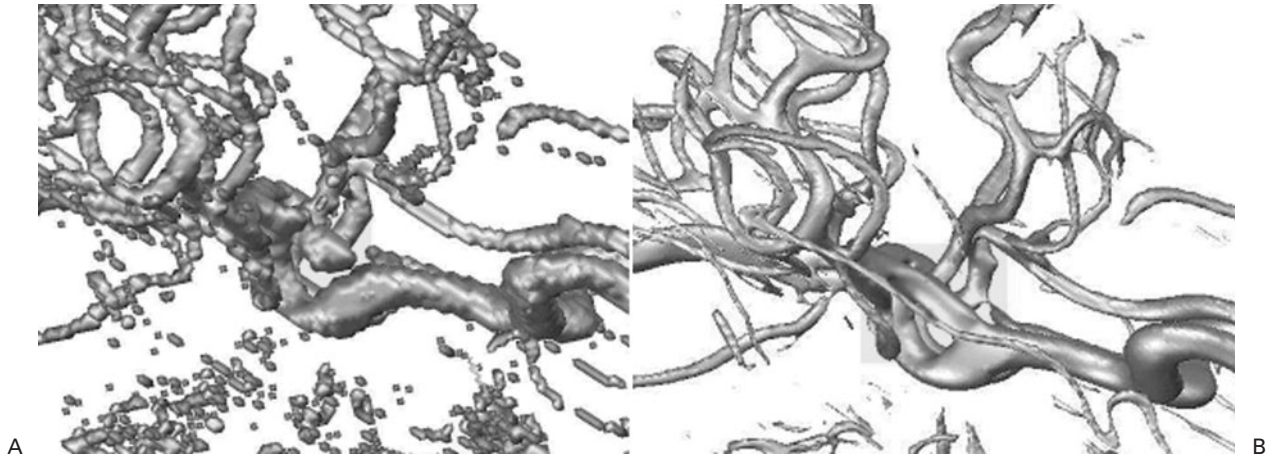
Figure 8 **MIP images of the circle of Willis in a patient with an aneurysm of posterior communicating artery on the left side of a female patient (62 years old), symptomatic with ICB.** (A) **MIP images of conventional MRA (lateral view);** (B) **MIP images of post-processed MRA (lateral view)**

complex was improved considerably: the vessels were displayed in a much smoother way. Artifacts and disturbing gaps were virtually reduced due to the effect of this new denoising method, and it produced an enhanced vessel representation. The visualization of the posterior circulation, particularly of the posterior communicating artery was much poorer in conventional MRA and in post-processed MRA, the sensitivity of post-processed MRA even being as low as 70% when compared with DSA. The results are similar to those published by Katz *et al.*[17] and by Stock *et al.*[8]. False-negative findings in MRA can result from turbulence and saturation effects of slow-flowing blood or long in-plane flow[8]. Relating to the poor sensitivity of post-processed MRA, one cannot expect a display of a vessel, which is not visualized in the original MRA image data. In case of a very poor signal intensity, a vessel could not be visualized after processing with anisotropic curvature motion. In case of a very poor signal intensity of a vessel in the original MRA image data, it will be assessed as an artifact in the post-processed MRA imaging. Furthermore, during the post-processing with the anisotropic curvature motion, the vessels have to be extracted from the original image first. This is carried out by a simple thresholding method[9]. Although this will not always be a reliable way of finding initial segmentations, we confine to this method for the application case study provided here. Thus, to obtain more reliable results, one should apply alternative methods for this first step of the process.

The post-processed MRA was able to demonstrate the aneurysm in four of the five patients. In one patient, an aneurysm of the posterior circulation was visualized as a "nonsense" communication between the posterior communicating artery and the ICA. In this case, the denoising method for restoring the 3D MRA designed bridging gaps in the wrong place. Concerning this particular problem, this method has to be optimized. It should be analysed how many cycles of post-processing are necessary to obtain or to improve definitely the smoothness of the vessels but avoid false bridging gaps.

In general, the presented post-processing method provides an infinite array of projections, including surgical views, of 3D images of the surgical anatomy because of viewing the cerebral arteries with a novel concept in 3D image that always provides an easy handling of 3D images.

Generating 3D images is possible with up-to-date modern post-processing methods and facilitates improved and smoothed representation of the neu-rovascular features of the circle of Willis. One should keep in mind the potential pitfalls of these methods in its present state and always double-check the final results with the original source or MPR images.

References

1 Wilcock D, Jaspan T, Holland I, *et al*. Comparison of magnetic resonance angiography with conventional angiography in the detection of intracranial aneurysms in patients presenting with subarachnoid haemorrhage. *Clin Radiol* 1996; **51**: 330–334

2 Leffers AM, Wagner A. Neurologic complications of cerebral angiography. A retrospective study of cerebral angiography. A retrospective study of complication rate and patient risk factors. *Acta Radiol* 2000; **41**: 204–210

3 Velthuis BK, Van Leeuwen MS, Witkamp TD, *et al*. Computerized tomography angiography in patients with subarachnoid hemor-rhage: From aneurysm detection to treatment without conven-tional angiography. *J Neurosurg* 1999; **91**: 761–767

4 Villablanca JP, Martin N, Jahan R, *et al*. Volume-rendered helical computerized tomography angiography in the detection and characterization of intracranial aneurysms. *J Neurosurg* 2000; **93**: 254–264

5 Villablanca JP, Jahan R, Hooshi P, *et al*. Detection and characterization of very small cerebral aneurysms by using 2D and 3D helical CT angiography. *AJNR Am J Neuroradiol* 2002; **23**: 187–1198

6 Kouskouras C, Charitanti A, Giavriglou C, *et al*. Intracranial aneurysms: Evaluation using CTA and MRA. Correlation with DSA and intraoperative findings. *Neuroradiology* 2004; **46**: 842–850

7 Tang BT, Cheng CP, Draney MT, *et al*. Abdominal aortic hemodynamics in young healthy adults at rest and during lower limb exercise: Quantification using image-based computer model-ing. *Am J Physiol Heart Circ Physiol* 2006; **291**: 668–676

8 Stock KW, Wetzel S, Kirsch E, *et al*. Anatomic Evaluation of the circle of Willis: MR angiography versus intraarterial digital subtraction angiography. *AJNR Am J Neuroradiol* 1996; **17**: 1495–1499

9 Nemitz O, Rumpf M, Tasdizen T, *et al*. Anisotropic curvature motion for structure enhancing smoothing of 3D MR angiography data. *J Math Imaging Vision* 2007; **27**: 217–229

10 Meyer M, Kirby M, Whitaker R. Topology, accuracy, and quality of isosurface meshes from dynamic particles. *Vis Comput Graph* 2007; **13**: 1704–1711

11 Clarenz U, Dziuk G, Rumpf M. On generalized mean curvature flow in surface processing. In: Karcher H, Hildebrandt S, eds. *Geometric Analysis and Nonlinear Partial Differential Equations*, Berlin: Springer, 2003: pp. 217–248

12 Andrews B. Volume-preserving anisotropic mean curvature flow. *Indiana Univ Math J* 1991; **50**: 783–827

13 Huisken G. Flow by mean curvature of convex surfaces into spheres. *J Differ. Geom* 1984; **20**: 237–266

14 Clarenz U, Rumpf M, Telea A. Robust feature detection and local classification for surfaces based on moment analysis. *IEEE Trans Vis Comput Graph* 2004; **10**: 516–524

15 Adalsteinsson D, Sethian JA. A fast level set method for propagating interfaces. *J Comput Phys* 1995; **118**: 269–277

16 Harrison MJ, Blake AJ, Gilbert MG, *et al*. Preliminary results on the management of unruptured intracranial aneurysms with magnetic resonance angiography and computed tomographic angiography, *Neurosurgery* 1997; **40**: 947–955

17 Katz DA, Marks MP, Napel SA, *et al*. Circle of Willis: evaluation with spiral CT angiography, MR angiography and conventional angiography. *Radiology* 1995; **195**: 445–449